

1 of 1

## CONCEPTS TO MEASURE FLUX AND TEMPERATURE FOR EXTERNAL CENTRAL RECEIVERS

**James E. Pacheco and Richard M. Houser**  
Solar Thermal Technology Department  
Sandia National Laboratories  
Albuquerque, New Mexico

**Andreas Neumann**  
Energy Technology Division  
Deutsche Forschungsanstalt für Luft- und Raumfahrt  
Cologne, Germany

### ABSTRACT

Three concepts to measure incident flux (1) relative, real-time power measurement, 2) flux mapping and incident power measurement, and 3) real-time flux mapping) and two concepts to measure receiver surface temperatures (1) low and 2) high resolution temperature measurements) on an external central receiver are discussed along with the potential and shortcomings of these concepts to make the desired measurements and the uncertainties associated with the measurements caused by atmospheric and surface property variations. These concepts can aid in the operation and evaluation of the receiver and plant. Tests have shown that the incident flux distribution on a surface can be mapped out using a fixed, narrow white target and a CCD camera system by recording the images of the beam as it is passed over the target and by building a composite image. Tests with the infrared cameras have shown they are extremely valuable tools in determining temperature profiles during startup of the receiver and throughout operation. This paper describes each concept in detail along with the status of testing to determine the feasibility of these concepts.

### INTRODUCTION

In a solar central receiver configuration, heliostats redirect and concentrate the beam component of sunlight onto a receiver mounted on top of a tower centrally located in the field of heliostats. The concentrated radiant power is absorbed by the receiver and transferred to fluid pumped through the receiver. The fluid collects the concentrated solar energy which is converted into work, then electricity, or for use as heat. Molten salt has been used extensively as the heat transport fluid in central receiver systems. In the Solar Two project (a cost-shared project between a consortium of utilities headed by Southern California Edison and the US Department of Energy), the central receiver power plant located near Barstow, CA will be retrofitted with an advanced molten-salt heat transfer system. The receiver will be an external cylindrical configuration made with tubes

that are painted black. With an external cylindrical receiver geometry, measurements of flux and temperature introduce unique challenges and needs. Measurements of the distribution of incident radiant flux, the total power going into the receiver, and the receiver surface temperature will provide important data that can aid in the operation, evaluation, analysis, and control of the receiver. These measurements can also help assure warranty conditions associated with the receiver and heliostat field are met. The objective is to evaluate concepts to measure flux and temperature and to determine their applicability to external cylindrical central receivers.

### DESCRIPTION OF THE CONCEPTS, UNCERTAINTY ANALYSES, AND TESTING

The spectrum of the radiant energy to be measured can be broken into two parts: the concentrated solar spectrum where the wavelength region of concern is usually between 0.3 to 4.0  $\mu$ m and the infrared (but not the solar radiation) whose wavelength region depends on the temperature of the surface of interest and is usually greater than 1.8  $\mu$ m for the temperatures associated with central receivers. A plot of the solar spectrum and two blackbody spectrums at the receiver inlet and outlet molten salt temperatures are shown in Figure 1.

Table 1 is a summary of each concept and instrumentation along with the positive and negative features. Each of these measurements requires specialized instrumentation to carry out the intended function. The measurements are listed in order of their importance and impact on the operation, maintenance, or reliability of a central receiver power plant and their ability to aid in assessing the performance of the receiver. The sections below describe each concept along with the uncertainty of the measurements and testing of the concepts. As of this writing, some of testing described below is underway at the Central Receiver Test Facility (CRTF) at Sandia National Laboratories. A brief description of the status and results of the testing are also described in these sections.

**MASTER**

James E. Pacheco

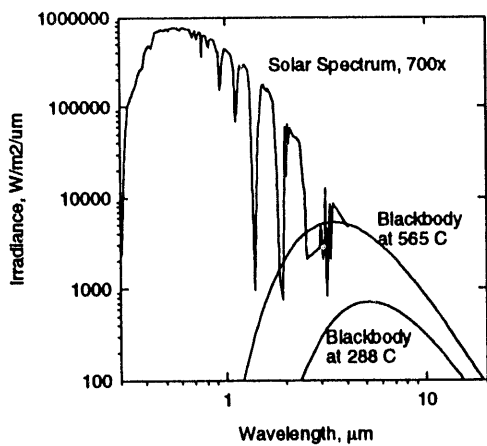


Figure 1. Terrestrial solar spectrum  $\times$  700 at air-mass 1.5 and two blackbody emission spectra.

#### Relative Power Measurement.

Reliable measurement of incident power is necessary to provide a feed-forward control signal to the molten-salt control system (Kolb, 1992). Receiver control systems have relied on the flux gauges to sense changes in flux on the receiver. Although these flux gauges have worked in central receivers with some success, they suffer from reliability problems, require frequent maintenance and calibration, and can be difficult to access. In the Solar One receiver - a single-pass-to-superheat boiler, 6.6% of the plant outages caused by the receiver were due to the flux gauges (Kolb and Lopez, 1988). These outages amounted to 3.4% of total plant outages. Experience has shown that the average life of a flux gauge in the harsh, concentrated solar environment is about 6 months. In order to mitigate plant outages due to failure of flux gauges, a strategy was proposed where one of the two flux gauges in a panel is replaced at three month intervals, staggering the replacement.

The flux sensor needs to respond rapidly enough to changes in incident power - such as those experienced in cloud transients - so the flow rate can be increased rapidly to cool the receiver and prevent overheating of the receiver tubes. The costs and maintenance requirements for flux gauges in a commercial plant are high enough that the development of highly reliable, low maintenance alternatives could have an immediate, positive effect on the maintenance costs and reliability of the receiver. The cost of the photometers is relatively low (~\$600 each).

Potential alternatives to flux gauges are photometers which do not sit in the high flux area of the receiver, don't have significant drift with time, can easily be maintained, and are low cost. Changes in incident power would be detected by measuring changes in reflected intensity. Several of these photometers would be mounted around the base of the receiver, each "seeing" a portion of the receiver not having a field of view so large that it picks up stray light or direct solar irradiance. A schematic of this arrangement in shown in Figure 2.

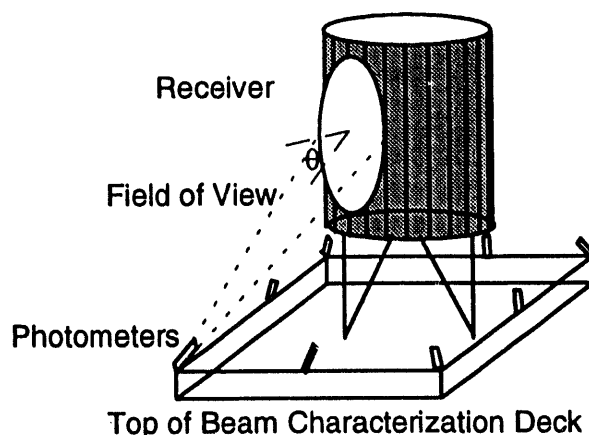


Figure 2. Schematic of arrangement of photometers to measure changes in relative power.

The photometers respond to reflected light over a region of the receiver whose view size is a function of the field of view and respond to light whose spectral content lies within the detection band of the photometer. The spectral content of the reflected light is a convolution of the beam component of terrestrial solar radiation, the spectral reflectivity of the heliostats, and the spectral reflectivity of the flat black absorber paint. Since the surface reflectivity will vary as the paint ages, the dynamic range of the photometers must be wide enough to accommodate these changes.

Uncertainty Analysis of Relative Power Measurement with Photometers. Photometers used to measure relative power for flow control need only to sense *changes* in reflected power to provide a feed-forward signal to the control system. The largest uncertainty associated with this measurement is that associated with Pyromark reflectivity. Since the photometers view a wide area of the receiver and since the solar-weighted absorptivity and thus reflectivity change slowly over time, bulk changes in reflectivity are manageable. After the Solar One receiver had been repainted with Pyromark in December 1985 it had an absorptivity of 97%. In October 1987 the absorptivity changed to 96% (Radosevich, 1988), showing that the properties change slowly with time. A calibration algorithm could be implemented to automatically account for changes in bulk reflectivity by scaling the photometer output signal to match the relative power on the receiver. For example, near solar noon on a clear day (or more often if necessary) under steady conditions when full power is known to be incident on the receiver, the scale factor for the photometers output signal could be reset to 100% relative power to account for minor variations in reflectivity.

Testing of Photometers. A test setup consisting of two receiver panels has been installed at the CRTF to test photometers and compare their output to flux gauges. To control the salt flow rate, the photometers must be able to respond to changes in incident flux as measured by the reflected light from the panels. In these tests, the photometer's response will be compared to flux gauge output using the setup shown in Figure 3. The goal is to determine how well the photometers can measure changes in flux compared to flux gauges and to

Figure 10.10 | Prevalence of the most common types of food poisoning in the United States.

Let us now turn to the analysis of the system with power  $W$ , which is the system with the additional term  $W \delta_{ij} \partial_i \partial_j$  in the right-hand side of (2.1). The corresponding system of equations is given by (2.1) with the right-hand side (2.2) replaced by

Digitized by srujanika@gmail.com

Table 4. Number of participants in each of the four groups in each of the four time points of the study.

$$T_{\text{min}}(T_{\text{max}}) = \left\{ \frac{1}{2} \left( \frac{1}{2} + \frac{1}{2} \text{erf} \left( \frac{T_{\text{min}}(T_{\text{max}})}{\sqrt{2} \sigma} \right) \right) \right\}_{\sigma=0}^{\sigma \rightarrow \infty} = \frac{1}{2} \left( \frac{1}{2} + \frac{1}{2} \text{erf} \left( \frac{T_{\text{min}}(T_{\text{max}})}{\sqrt{2} \sigma} \right) \right)_{\sigma=0}^{\sigma \rightarrow \infty}$$

<sup>14</sup> See, for example, the discussion of the 'right to be forgotten' in the European Union's General Data Protection Regulation (GDPR), Article 17(1).

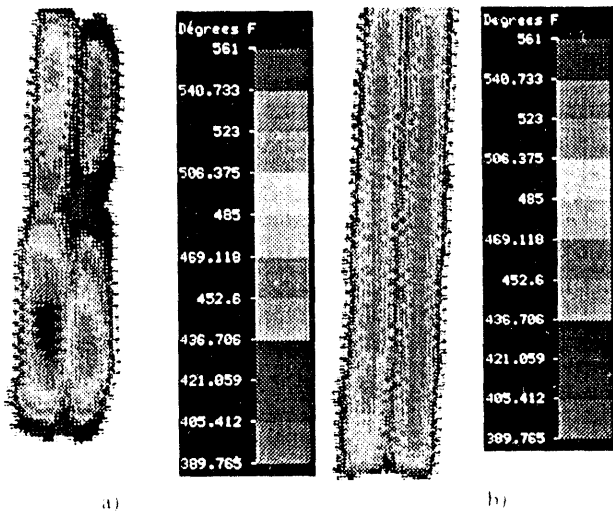


Figure 5 Thermal image of panel a) preheated with heliostats and b) after flow was established bringing the panel to an equilibrium temperature

Errors introduced in the measurement are caused by absorption and scattering of radiation by air, reflection from nearby hot objects, emissivity variations, and reflection of concentrated sunlight. The error in temperature measurement due to absorption of radiation through air is proportional to the optical path length - the distance between the hot surface and the detector. At 100 meters from the surface at 800°C and an atmospheric transmission of 95.3%, the atmospheric absorption will cause an error of 14°C. This error increases to 23°C for a transmission of 92.3% (Neumann, 1993). For back surfaced glass silvered mirrors, the solar noise or "pollution" of the IR signal is small in the 8-12  $\mu\text{m}$  range since the glass absorbs most of the light in this wavelength band. A 5% change in emissivity will result in an underestimation by about 23°C at an operating temperature of 650°C and is additive to the other errors. Phipps and Sweatt (1992) have proposed using bandpass filters at selective wavelengths to minimize effects of atmospheric conditions and solar "pollution".

The emissivity correction can be made in the field during startup by viewing the receiver just after salt flow has been initiated but prior to heat collection. The receiver should be at a fairly uniform, known temperature during this startup phase - the salt inlet temperature - so the emissivity can be adjusted to match that temperature.

**Testing of Low Resolution IR Camera.** Tests were performed with two panels used in a molten salt panel experiment located at the base of the CRIE. The panels were heated with heliostats and after they reached a temperature near the salt temperature, flow was initiated through the panel tubes. Thermal images were captured using two Inframetrics cameras. Two of the images are shown in Figures 5a) and 5b) where the panel was preheated with heliostats, and after flow was established through the entire panel, respectively.

Since the real receiver emissivity will vary with location, one method to measure this variation is to measure the emission

from a surface at uniform temperature. At a uniform temperature, a surface that has significant *spatial* variation in emissivity will appear to have a spatial variation in temperature when viewed by the IR camera. After flow was established in the two panels in the molten salt loop, the panel temperature became very uniform and equilibrated at the salt temperature. By viewing the panel with the IR cameras, we determined that the spatial variations in emissivity were not significant and did not adversely affect the temperature measurement. We observed there was no noticeable solar interference in the measurements, but the solar intensities were very low ( $< 30 \text{ kW/m}^2$ ).

The biggest advantage of this thermal imaging system is that the flow condition within the panel can be determined. As the receiver panel filled with salt, we could "see" the salt/air interface. During one of our molten salt panel tests, some of the passes were blocked by air trapped in the flow path. Using the IR cameras we were able to determine which tubes had blockage. In a commercial power plant, this information could be invaluable, especially if the receiver were to become frozen with salt.

#### High Accuracy Flux Mapping and Total Incident Power Measurement on Receiver.

High precision and accurate measurements of the incident flux and total power from the entire heliostat field are very important for assessing receiver performance. This system would provide valuable insight on the actual flux distributions on the receiver and could aid in optimizing heliostat aiming strategies in addition to being used to measure incident power for receiver efficiency calculations. A major concern in a commercial scale, central receiver plant is how the heliostat field and receiver subsystems are warranted. If the heliostat field is provided by a different supplier than the receiver vendor, the question arises - who warrants the thermal performance under given conditions? A heliostat manufacturer may guarantee a specific power delivery to the receiver under predefined conditions and the receiver manufacturer may warrant a given thermal power output to the heat transport fluid given a power input at the receiver surface, but without knowing the incident power on the receiver the warranties might not be fulfilled.

In order to accurately measure the receiver efficiency, the total power onto the receiver must be known along with the power absorbed by the heat transport fluid (as measured by the flow rate and temperature rise of the fluid). A system to measure incident flux would consist of a video camera operating in the visible spectrum, a computer with a frame grabber and image processing software. The camera takes images of the white target which is placed in the beam. The target must be coated with a high quality white diffuse reflective material (e.g., aluminum oxide, magnesium oxide, or others). This type of system can be realized in different ways. The Beam Characterization System (BCS), (Thalhammer, Phipps, 1979) used at the Central Receiver Test Facility (CRIE) in Albuquerque, NM, operates with a large white target on the receiver tower. The beam of a single heliostat or several of them are characterized by images taken on that target. The beams could then be moved on to the receiver. The HERMES II

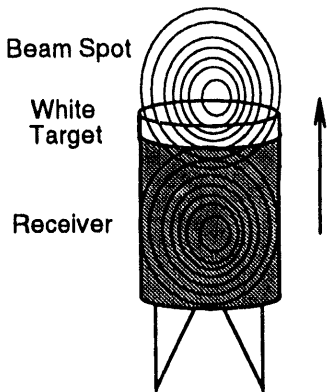


Figure 6. Fixed Lambertian target for measuring flux distribution on central receiver. The heliostat beams are moved up and across the narrow target to map out the flux.

System developed by the DLR in Cologne, Germany, and operated at the Plataforma Solar in Spain uses a narrow elongated rectangular white target (Neumann, 1991). This target sweeps across the front of the receiver aperture to scan the entire beam. The new solution proposed here is a combination of the two principles. A narrow white target coated with a highly reflective material is mounted on top of the receiver. Figure 6 shows a schematic of this arrangement. Instead of moving a target in front of the receiver, the beam itself is swept across the target. By incrementally moving the aim points of the heliostats upwards, the heliostat beams pass over the white target to map out the flux distribution. The images could then be cropped, rectified, and a composite image of the flux distribution of the entire receiver could be built. The narrow target requires less cooling power than a large target would need for taking complete images of the heliostats. Provided there is nothing above the receiver expect the white target, the beams passing over the top of the tower and target cannot cause any heating damage. For that reason many heliostats can sweep simultaneously across the target.

A moving white target concept was ruled out as a way of mapping out the flux distribution because it would be impractical to be used in a large, external cylindrical receiver configuration. This system could also enable the operators to find the peak flux location to check aiming strategies. The number of cameras needed depends on how diffuse the white target is. Figure 7a) show the angular dependency of the reflectivity of  $\text{Al}_2\text{O}_3$  - a common coating for target surfaces. An ideal diffuse surface will scatter light equally in all directions. The  $\text{Al}_2\text{O}_3$  reflective surface behaves diffusely (Lambertian) over  $\pm 45^\circ$  (reflection angles) at all light incident angles presented. This means off-axis measurements of the flux from the white target can be made accurately and four to six cameras would be required.

Uncertainty Analysis of the High Accuracy Flux Mapping Concept. As solar radiation passes through the atmosphere it is attenuated and the spectral content of the radiation that reaches the surface of the earth is a function of the optical path length, aerosol scattering and absorption, water vapor absorption and transmittance through ozone and mixed gases in the atmosphere.

As these atmospheric constituents affect solar radiation, they will also influence remote optical measurements carried out in similar spectral regions. Since CCD video cameras measure radiant flux over a limited detection band width, the entire solar spectrum cannot be measured but must be inferred from the radiation that is detected. A typical CCD video camera measures visible radiation in the 0.3 to 1.1  $\mu\text{m}$  wavelength range. We used the SPCTRAL2 solar irradiance model (Bird and Riordan, 1986) which accounts for absorption and scattering of the previously mentioned parameters to calculate the ratio of irradiance in the wavelength range 0.3 to 1.1  $\mu\text{m}$  to that in the 0.3 to 4.0  $\mu\text{m}$  wavelength range (nearly all the solar spectrum). We found that variations in water vapor and turbidity do not change the ratio by more than about  $\pm 3\%$  for most conditions. During condition of high turbidities (low visibility) and at large zenith angles (near sunrise or sunset), the uncertainties grow larger than this, but these are unlikely conditions for measuring receiver performance. Phipps and Sweatt (1992) have proposed using a bandpass filter at 0.68  $\mu\text{m}$  with silicon detectors to minimize the effects of changing aerosol content on atmospheric transmission of visible light.

In addition to the effects on measurements of concentrated flux caused by atmospheric variations, the properties of the heliostat reflective surface, the spectral response of the detector, and the angular reflective properties of the target can also affect the remote measurements. The concentrated radiation reflected off a surface is a convolution of the terrestrial beam solar radiation, the heliostat reflectivity, and the surface reflectivity along with atmospheric absorption between the surface and the detector.

Factors that contribute to uncertainties in the measurement of flux for the fixed Lambertian target concept, are variations in atmospheric conditions ( $\pm 3\%$ ), absolute calibration of the intensity level ( $\pm 5\%$ ), camera linearity ( $\pm 1\%$ ), camera hardware including amplifier ( $\pm 1\%$ ) and digitizer ( $\pm 1\%$ ), and variations in the white target properties ( $\pm 4\%$ ). The root-mean-square uncertainty in this measurement is approximately  $\pm 7\%$ . Furthermore, since the camera intensity level is digitized, the dynamic range for an 8-bit digital system is 1 to 256. In addition to these errors, there can be errors introduced by displacement of the heliostat beam upward when the beam is being mapped out. This error will be greater for heliostats in the rows closest to the tower and least for ones at the edge. This error should be relatively small compared to the others. Heliostats near the singularity point may not be able to respond fast enough for this measurement.

Test of High Accuracy Flux Mapping with a Fixed Lambertian Target. Several tests were performed to test the feasibility of mapping out the flux distribution and determining the total power using a simulated narrow white target (smaller than the beam size). The actual target was in a bay of the CRTF and was large but only a section was of interest for postprocessing the image. In these tests, several heliostats were aimed at the target. The vertical heliostat aim points were incrementally moved upward over the target while the BCS (COHU CCD video camera with telescopic lens, 8-bit frame

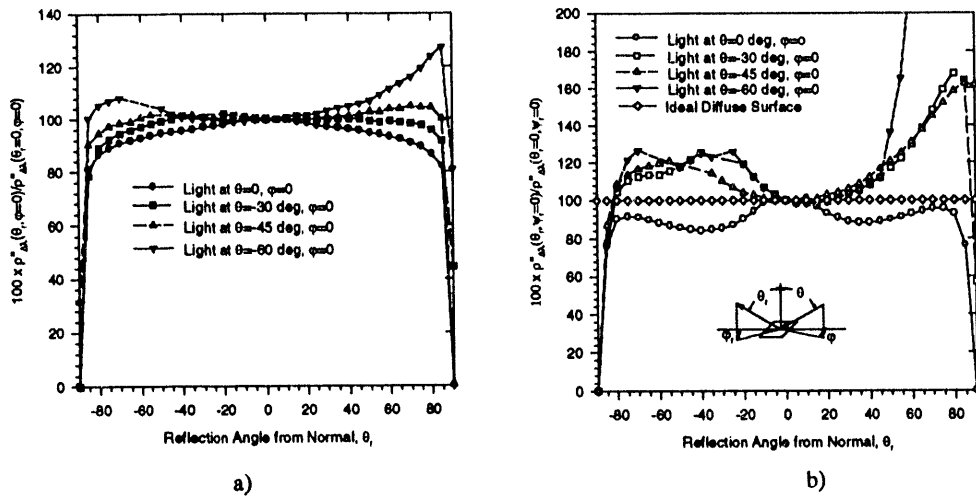


Figure 7. Normalized bi-directional reflectivity for a) plasma sprayed  $\text{Al}_2\text{O}_3$  and for b) Pyromark paint at various incident angles over the wavelength range 0.5-1.1  $\mu\text{m}$  using a tungsten lamp for the light source. Each curve (with a fixed, light incidence angle) is normalized by its reflectivity at zero incidence and is not normalized with the others.

grabber system, a 486 DOS computer system, and Beamcode software) captured the images of the beam reflected off the white target. A section of each image representing the narrow target whose height was the incremental distance between vertical aim points was cropped and merged to form a composite image of the entire beam. A typical result from these tests is shown in Figure 8 where 30 heliostats were aimed at a single, common aim point on the white ( $\text{Al}_2\text{O}_3$ ), water-cooled panel. The aim point was moved upward in 0.4 m increments to map out the 2.0 m beam spot. From a qualitative comparison, the composite image has similar contour profiles as the parent images. Analyses of the composite image indicated the total power, peak power, and beam size were within 2% of mean values of the individual images that made up the composite. The time required to move the heliostats from one aim point to the next and allow the heliostats to settle was approximately 15 seconds. To get the flux profile from a cylindrical target, the image would have to be rectified to account for the curvature.

#### Real-Time Flux Mapping Measurement

A warranty concern may arise if the integrity of the receiver were breached. The question could arise as to whether the flux on the receiver surface exceeded design limits - a heliostat field problem - or whether the receiver tube materials or receiver design or manufacturing was faulty - receiver problem. In addition, real time flux distributions on the receiver as it is operating can help to verify and optimized aiming strategies. Continuous measurements of the flux distribution need to be made in *real time*. The only practical method to measure the flux distribution continuously without interrupting the operation is to measure the reflected flux off the receiver surface with video cameras. This arrangement is similar to the one in Figure 6 except the cameras view the absorber panels directly and there is no need to move the heliostat aim points. Since the reflected light and thus the flux distribution measurements are very sensitive to changes in the spatial reflectivity, a calibration of the

receiver reflectivity must be made periodically in order to get meaningful data.

#### Uncertainty Analysis of Real-Time Flux Mapping Concept

The uncertainties associated with the real-time flux measurement concept are similar to those associated with the fixed Lambertian target concept except for the uncertainties of the surface reflectivity. The absorber paint reflectivity may vary significantly with location (spatially) on the receiver and will depend on the curing process and age of the paint. A change in solar-weighted absorptivity of the receiver surface from 95% to 94% results in a 20% change in reflectivity. Unfortunately these gross errors overwhelm all other uncertainties and make the flux mapping measurements only qualitative at best. It may be possible to build a calibration map of the receiver surface using a well-characterized heliostat or light source. Also, the directional properties of the Pyromark reflectivity must be considered. The absorber paint must be diffuse in order to make these measurements. Figure 7b) shows the directional reflective properties of Pyromark. The paint behaves fairly diffusely over the range of angles of interest ( $\pm 45^\circ$ ), but it exhibits higher reflectivity at the incident angle of the light source. The estimated uncertainty for this concept is  $\pm 20\text{-}40\%$ .

Testing of Real-Time Measurement of Flux Map Using Receiver Panels. These tests use the same two panels and setup in the photometer tests. The purpose is to determine the feasibility and limitations of measuring the reflected light off the receiver panels as a way of estimating the incident flux map in real-time. The flux profile can be measured first with white, water-cooled panels in another bay of the CRTF, then it can be compared to that from the receiver panels. Qualitative comparisons can be made of the profiles. Images will be captured with the same camera system as was used in the fixed Lambertian target tests. A procedure will be tested to estimate the variation in reflectivity over the receiver surface using either a well-characterized heliostat image or light source. A

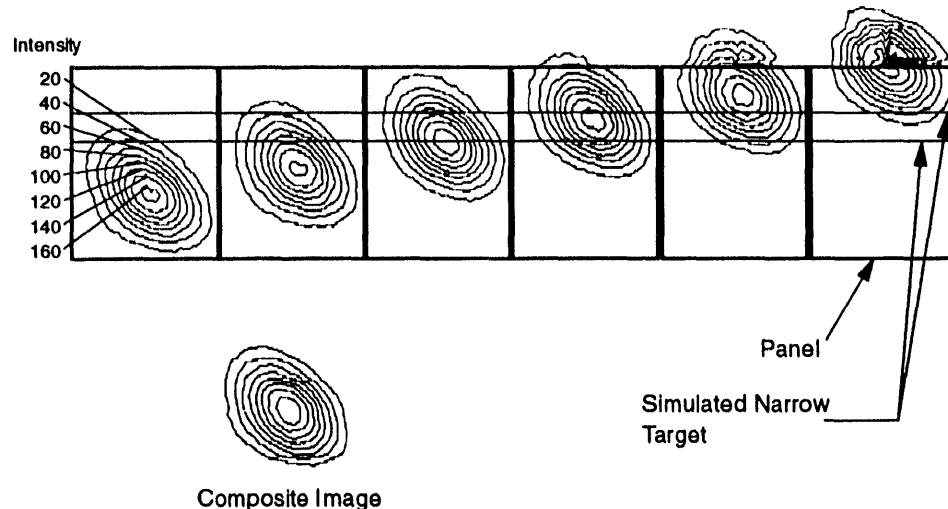


Figure 8. Isocontour plots of a beam spot from 30 heliostats from a test to simulate a fixed Lambertian target test. The rectangular boxes represent the white panel and the horizontal lines mark the sections where each image was cropped - simulating a 0.4 m narrow target and merged to form the composite image.

calibration map of the spatial receiver reflectivity can be developed to increase the accuracy of the flux measurement. The angle at which the camera views the panel can also be varied. These tests will be conducted using groups of heliostats over a range of flux levels.

#### High Resolution Temperature Measurement for Diagnostics

High spatial resolution temperature measurement of receiver tubes would enable the peak temperatures and temperature gradients across individual tubes to be measured. The highest flux levels are seen on the tube crown and drop off in the radial direction. The flux gradients across the front surface of the tube result in severe radial temperature gradients and thus radial stresses. Detailed resolution of temperature profiles across individual tubes could be used to assess tube stresses and to verify receiver designs and integrity. This system would require high spatial resolution. The measurements could be made using an infrared camera mounted close to the receiver, and fitted with the proper lens. This system would be installed as part of the diagnostics. Measurements from this system would enable valuable analysis of receiver tube stresses, but would not have a significant impact on the operation, maintenance, or reliability of the plant.

Uncertainty Analysis of High Spatial Resolution Temperature Measurement. The uncertainty of the temperature measurement with this concept should be at least as good as the low resolution temperature measurement system and it will likely be better with a calibration of the tube surface. Also, at close ranges (<10m), the effects of atmospheric absorption on the temperature measurement are not significant.

Testing of High Resolution Temperature Measurement. In these tests, we plan to examine the feasibility of using a CO<sub>2</sub> laser to calibrate the emissivity of tubes painted with Pyromark heated to the cold and hot salt temperatures. This calibration technique will enable us to obtain high accuracy temperature

measurement over small regions of interest on the receiver (Phipps and Sweatt, 1992). We will scan the sample with the laser and measure the reflected signal to estimate the emissivity.

If this calibration procedure proves acceptable, we can calibrate a region of the receiver panels and mount the same 8-12  $\mu$ m IR camera fitted with a lens close to the surface (<10m) to resolve the temperature across the crown of the tube. By heating the panels up dry, we can view the temperature profiles across the tube surface to determine how well they can be resolved.

#### **CONCLUSIONS**

Of the concepts proposed to measure flux and temperature on central receivers, the two that could have the greatest impact on the receiver reliability and the plant operation are the photometers for flow control and the low resolution IR cameras for measuring temperature profiles of the receiver during startup and operation. The low spatial resolution IR camera system has proven to be an extremely useful tool for aiding and understanding the operation of a receiver. The fixed Lambertian target concept shows promise as a way to map out the flux distribution on the receiver, however, it may be complicated to implement. With the large variations in the Pyromark reflectivity across the surface of a receiver, it is likely that measuring flux directly off the receiver surface will be qualitative at best. The high-resolution temperature-measurement system will be useful for analysis of the receiver stress, but may not significantly impact the operation or reliability of the receiver or plant.

#### **ACKNOWLEDGMENTS**

The authors would like to thank Bill Sweatt and Gary Phipps who provided valuable insight on measurements with infrared and visible video cameras and atmospheric and surface variables that affect the measurements, Rod Mahoney for making the

measurements of the Pyromark emissivity and sharing his experience with Pyromark paint, and Mark Nissen for carrying out the IR tests and data reduction. This work is supported by the U.S. Department of Energy under contract DE-AC04-76DP00789, SAND93-2504C.

94 AL 85000

## REFERENCES

Bird, R.E., C. Riordan, "Simple Solar Spectral Model for Direct and Diffuse Irradiance on Horizontal and Tilted Planes at the Earth's Surface for Cloudless Atmospheres", *Journal of Climate and Applied Meteorology*, Vol. 25, pp. 87-97, Jan. 1986.

Kolb, G. J., "Development of a Control Algorithm for a Molten-Salt Solar Central Receiver in a Cylindrical Configuration", *Solar Engineering*, Vol.-3, Proceedings from the 1992 ASME-JSES-KSES International Solar Energy Conference, pp. 1043-1051, Maui, HI, April 1992.

Kolb, G. J., C. W. Lopez, *Reliability of the Solar One Plant During the Power Production Phase*, Sandia National Laboratories, Albuquerque, NM, SAND88-2664, October 1988.

Neumann, A., "Proposal of a Rotatory Bar Movement", DLR/PSA Memorandum, Cologne/Tabernas, 1991.

Neumann, A., DLR Cologne, Germany, compiled from a seminar on the HERMES II system given in February 1993 and from personal communications at Sandia National Laboratories.

Phipps, G. S., and W. C. Sweatt, memo to J. M. Chavez, "Analysis of Desired Solar II Instrumentation", December 4, 1992.

Radosevich, L. G., *Final Report on the Power Production Phase of the 10 MW<sub>e</sub> Solar Thermal Central Receiver Pilot Plant*, Sandia National Laboratories, Livermore, CA, SAND87-8022, March 1988.

Thalhammer, E. D., G. S. Phipps, "Heliostat Beam Characterization System", Proceedings of the 25th International Instrumentation Symposium, Anaheim, CA, SAND79-0697, May 1979.

## DISCLAIMER

This report was prepared as an account of work sponsored by an agency of the United States Government. Neither the United States Government nor any agency thereof, nor any of their employees, makes any warranty, express or implied, or assumes any legal liability or responsibility for the accuracy, completeness, or usefulness of any information, apparatus, product, or process disclosed, or represents that its use would not infringe privately owned rights. Reference herein to any specific commercial product, process, or service by trade name, trademark, manufacturer, or otherwise does not necessarily constitute or imply its endorsement, recommendation, or favoring by the United States Government or any agency thereof. The views and opinions of authors expressed herein do not necessarily state or reflect those of the United States Government or any agency thereof.

Table 1. Summary of Details of Instrumentation, Advantages, Disadvantages of Concepts to Make Measurements.

Measurement	1.) Relative Power Measurement	2) Low Resolution Global Temperature Measurement	3 a) High Precision Flux Mapping and Total Incident Receiver Power Measurement	3 b) Real-Time Flux Mapping and Total Incident Receiver Power Measurement	4) High Resolution temperature measurement
Function or Use	Feed-forward flow control signal, alternative to flux gauges	Receiver startup, thermal performance, and warranty concerns.	Performance assessment, accurate measurement of total power and flux.	Satisfy warranty concerns (real-time flux map). Verify heliostat aiming.	Tube crown temperature to aid in thermal strain analysis (diagnostics).
Instrumentation	6-8 silicon or thermopile type photometers mounted near receiver	4 infrared video cameras (field mounted) with hardware and imaging software	4 (CCD) video cameras (field mounted) with hardware, imaging software and a fixed white Lambertian target	Same as 3 a) but uses receiver surface as the target	1 infrared camera with 10 cm lens mounted near receiver surface
Wavelength Band of Detection	0.3-1.1 $\mu\text{m}$ (silicon) or 0.3-4.0 $\mu\text{m}$ (thermopile)	8-12 $\mu\text{m}$ or a wavelength band in that range	0.3-1.1 $\mu\text{m}$ or a single wavelength band within this region	Same as 3 a)	8-12 $\mu\text{m}$ or a wavelength band in that range
Measurement Range	0-100% Relative Power 6° field of view resolution	200-500°C 0.5 m spatial resolution	10-800 $\text{kW/m}^2$ 10 cm spatial resolution	Same as 3 a)	200-650°C 3 mm spatial resolution
Accuracy	$\pm 15\text{-}20\%$ with calibration	$\pm 30^\circ\text{C}$ with emissivity calibration	$\pm 7\%$ depending on calibration method	$>\pm 20\text{-}40\%$ due to large variations in receiver reflectivity	$\pm 30^\circ\text{C}$ with emissivity calibration
Positive Features	High reliability, low cost, easily to access & maintain, accurately detect changes in power	Very useful tool for monitoring receiver thermal condition. Commercially available	Based on BCS technology. Can verify aiming strategies. Relatively low cost. White target is simple to design and fabricate	Real time measurements. No target is required. No interruption of receiver operation.	Measure temperature variation across tube crown.
Negative Features	Sensitive to changes in bulk receiver surface reflectivity which changes significantly, but slowly with age	Very high cost. Delicate instrument. Requires cooling. Sensitive to atmospheric conditions and emissivity.	Not real time measurement. Special software required. Interrupts receiver operation. Target needs cooling.	Accuracy is poor - dependent on reflectivity of surface which varies with location and age.	High cost. May require special calibration methods to measure emissivity.
Comments	Simple calibration method may correct slow changes in reflectivity over field of view	Method to correct emissivity may be done simply during receiver start up after salt flow is established	Easiest way to accurately map out receiver flux distribution	Receiver reflectivity calibration map may improve accuracy. Only method to get continuous flux map measurements.	Part of diagnostics to assess tube stress. Will not aid in the operation or reliability of receiver.

11/14/94

2/14/94

FILED

DATE

